DOI: 10.1002/ejic.200901027

Mixed Tellurides $Ni_{3-x}GaTe_2$ ($0 \leq x \leq 0.65$): Crystal and Electronic Structures, Properties, and Nickel Deficiency Effects on Vacancy Ordering

Anna A. Isaeva,*[a,b] Olga N. Makarevich,[c] Alexey N. Kuznetsov,[b] Thomas Doert,[d] Artem M. Abakumov,[a,b] and Gustaaf Van Tendeloo[a]

Keywords: Nickel chalcogenides / Subvalent compounds / Electron microscopy / NiAs derivatives / Layered compounds

The $Ni_{3-x}GaTe_2$ series of compounds ($0 \leq x \leq 0.65$) was synthesized by a high-temperature ceramic technique at 750 °C. Crystal structures of three compounds in the series were determined by X-ray powder diffraction: $Ni_{2.98(1)}GaTe_2$ (R_I = 0.042, R_p = 0.023, R_{wp} = 0.035), $Ni_{2.79(1)}GaTe_2$ (R_I = 0.053, R_p = 0.028, R_{wp} = 0.039), $Ni_{2.58(1)}GaTe_2$ (R_I = 0.081, R_p = 0.037, R_{wp} = 0.056); the structures were verified by electron diffraction and, for the former compound, high-resolution electron microscopy. The compounds crystallize in a hexagonal lattice with $P6_3/mmc$, and the structures can be regarded as a hexagonal close-packed array with a –Ga–Te–Te– stacking sequence. The octahedral and trigonal bipyramidal voids in the *hcp* structure are selectively filled with Ni atoms to form one entirely occupied and two partially occupied sites, thus allowing variations in the nickel content in the series of compounds $Ni_{3-x}GaTe_2$ ($0 \leq x \leq 0.65$). A superstructure with $a_{sup} = 2a_{sub}$ ($P6_3/mmc$) has been identified for $Ni_{3-x}GaTe_2$ ($0.5 \leq x \leq 0.65$) by electron diffraction. Real-space, high-resolution images confirm an ordering of Ni atoms and vacancies in the *ab* plane. Quantum-chemical calculations performed for $Ni_{3-x}GaTe_2$ (x = 0, 0.25, 0.75, 1) suggest anisotropic metallic conductivity and Pauli paramagnetic behavior that are experimentally confirmed for Ni_3GaTe_2.

Introduction

Over recent years, nickel has proven to be a source of many interesting structures that feature low-dimensional heterometallic nickel–main-group metal fragments in nonmetallic matrices.[1] Such structural peculiarities give rise to a structural anisotropy and provide the basis for potentially applicable physical properties, such as anisotropic electric conductivity or low-dimensional magnetism etc.

Several recent investigations undertaken for the ternary T–M–Te systems (T = Ni or Fe; M = p-element of groups 13–15) revealed a number of layered mixed tellurides with the general formula $T_{3-x}MTe_2$, namely Ni_2SbTe_2,[2] $Ni_{2.95}GeTe_2$,[3] $Fe_{2.83}GeTe_2$,[3] $Ni_{2.58}SnTe_2$,[4] and $Ni_{2.87}SnTe_2$.[5] All these compounds contain structurally similar two-dimensional fragments of the NiAs or defective Ni_2In type, with heterometallic bonding between the transition and main group metals that extend in the *ab* plane, and are terminated along the *c* axis by Te atoms that form a van der Waals gap (Figure 1). The crystal structure of $T_{3-x}MTe_2$-type compounds can be regarded as a derivative of the NiAs motif, with its unit cell parameter *c* tripled with respect to that of the NiAs subcell (see Figure 1). This superstructure is generated by both main group elements to form an *hcp* array with an ordered –M–Te–Te– stacking sequence along the *c* axis. A partial occupancy of trigonal bipyramidal **A** and octahedral **B** voids (see Figure 1b) within the array results in d-metal compositional nonstoichiometry, characteristic for these compounds. In addition, ordered solid solutions $Ni_{3+x}In_{1-y}Te_{2+y}$ adopt very similar structures for x = 0.12, 0.32 and $y \approx 0$,[6] although the authors propose an intermixed occupancy of In and Te sites, which leads to a deviation from the 1:2 ratio between the main group metal M and Te and makes the metallic and chalcogenide parts of the structure less distinguishable (an effect that has not been reported for other similar compounds).

We have conducted a further search for new $Ni_{3-x}MTe_2$-type compounds for the "lighter" p-elements of groups 13–15. A systematic analysis of their structural similarities and differences could help to gain an insight into the crystal chemistry of low-dimensional transition metal/main group element bond systems. In the present work, we report the results of a systematic study performed on the systems Ni–M–Te (M = Al, Ga, Si, As), which led to the discovery of the $Ni_{3-x}GaTe_2$ ($0 \leq x \leq 0.65$) series of compounds. Note that we previously reported on the existence of Ni_3GaTe_2, which crystallizes in the hexagonal system with unit cell parameters a = 3.9378(2) Å, c = 15.775(1) Å in a short com-

[a] EMAT (Electron Microscopy for Materials Science), Physics Department, University of Antwerp
Groenenborgerlaan 171, 2020 Antwerp, Belgium
Fax: +32-3-265-33-18
E-mail: anna.isaeva@ua.ac.be
[b] Inorganic Chemistry Division, Chemistry Department, Moscow State University
Leninskie Gory, 1/3, 119991 Moscow, Russia
[c] Materials and Technology Research and Engineering Center, 2nd Baumanskaya street, 9/23, 105005 Moscow, Russia
[d] Dresden University of Technology, Department of Chemistry and Food Chemistry, Helmholtzstraße 10, 01062 Dresden, Germany

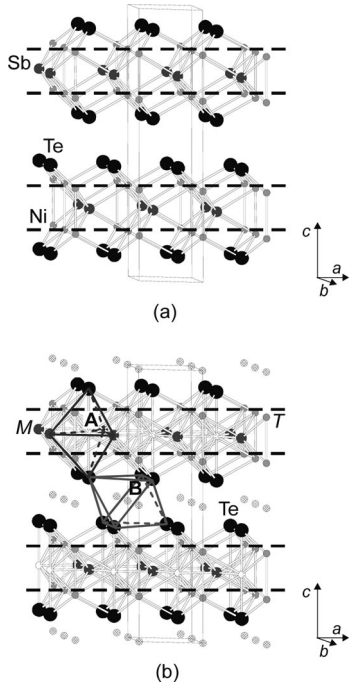

Figure 1. A general view of the $T_{3-x}MTe_2$-type structure (T = Ni, Fe; M = In, Ge, Sn, Sb). Dashed lines outline the borders of the 2D heterometallic T/M slab. **A** denotes the d-metal site within the heterometallic fragment that is partially occupied for all compounds, with the exception of Ni_2SbTe_2 (a). A van der Waals gap can be either empty for $Fe_{2.83}GeTe_2$, Ni_2SbTe_2 (a) or partially filled by extra Ni atoms in the **B** site for $Ni_{2.95}GeTe_2$, $Ni_{3-x}SnTe_2$ (b).

munication,[4] but no structural data and homogeneity range with respect to the nickel content were given. We have now investigated the whole range of compositions for $Ni_{3-x}GaTe_2$ from $x = 0$ to $x = 1$ and identified a superstructure that stabilizes Ni-poor compositions. This ordering was not previously found for any $Ni_{3-x}MTe_2$ compound and is directly connected to a selectivity of the filling of the nickel sites.

Results and Discussion

Sample Characterization

According to the phase analysis results, both samples with the starting compositions 2Ni+Ga+2Te and 3Ni+Ga+2Te after annealing represent a new ternary phase – their X-ray patterns are very similar to those of known $Ni_{3-x}MTe_2$ compounds. The Ni-rich sample was found to be phase-pure and homogeneous, which allowed us to assume that a single Ni_3GaTe_2[4] phase was prepared. The annealing period required to achieve phase equilibrium can be reduced by starting from binary telluride and elements rather than from the elements only. Single-phase powder samples were then prepared starting from a mixture of presynthesized Ga_2Te_3, Ni, and Te by annealing at 750 °C for 5 days.

The Ni-poor sample also contained the ternary phase – its reflections are shifted towards lower 2θ angles with respect to Ni_3GaTe_2 – along with admixtures of Ga_2Te_3 and $Ni_{1-x}Te$. The latter two could not be removed by successive annealing at 750 °C or higher temperatures for a period of up to 2 weeks.

EDX analysis performed on a number of crystallites, extracted from product batches, yields an overall composition of $Ni_{2.3(1)}GaTe_{1.9(1)}$ (averaged over 40 crystallites) for the Ni-poor sample and $Ni_{3.1(1)}GaTe_{2.0(2)}$ (averaged over 30 crystallites) for the Ni-rich sample, which agrees well with results of EDX analysis reported previously.[4] No discrepancies in the nickel content for Ni_3GaTe_2 were observed for both synthesis routes.

All other samples synthesized in the Ni–M–Te (M = Al, Si, As) ternary systems consisted of known phase mixtures: Ni, NiTe, and NiAl for the 2Ni+Al+2Te starting composition; Ni, NiAl, Ni_5Al_3, and NiTe for the 3Ni+Al+2Te starting composition; NiSi and $NiTe_2$ for the 2Ni+Si+2Te starting composition; Ni_3Si_2 and $Ni_{1-x}Te$ for the 3Ni+Si+2Te starting composition; NiAs and $NiTe_2$ for the 2Ni+As+2Te starting composition; $Ni_{1-x}Te$ and $Ni_{11}As_8$ for the 3Ni+As+2Te starting composition. Their phase compositions are in full agreement with equilibrium phase relations in the respective systems.

Furthermore, in order to investigate the effect of the Ni content on the crystal structure, a series of $Ni_{3-x}GaTe_2$ compounds with different compositions ($x = 0.25$, 0.5, 0.7, 0.75) was prepared. According to the XRD data, the two most Ni-deficient samples with $x = 0.7$ and 0.75 contain admixtures of Ga_2Te_3 (ca. 5%), while the others are obtained as single-phase samples.

The XRD patterns for all $Ni_{3-x}GaTe_2$ ($x = 0$, 0.25, 0.5, 0.7, 0.75, 1) samples are indexed in a primitive hexagonal unit cell with lattice parameters listed in Table 1. According to the EDX measurements, the compositions of the crystallites varied from the nominal composition of the batch in the case of Ni-poor samples with $x = 0.7$, 0.75, 1, consistently showing a slightly higher nickel content and attaining an approximate composition $Ni_{2.35}GaTe_2$ (see Table 1). The variations in the parameter a are minor, while the parameter c apparently decreases as the Ni content increases. The data for the unit-cell parameters and the elemental composition of Ni_3GaTe_2 are consistent with those published previously,[4] thus showing that the nickel content is nicely reproduced despite the differences in preparation conditions.

The products of the crystal growth experiments either without flux material or with a NaCl flux contain a large number of golden hexagonal crystals. In both cases, these crystals were identified by EDX as $Ni_{3.0(1)}GaTe_{2.0(2)}$.

Some crystals from both batches were tested on a Stoe IPDS-2 or a Bruker Kappa Apex 2 automated diffractometer, equipped with area detectors, but none were found to be suitable for crystal structure determination: the indexing and integration of the collected data were not possible, probably because of the effects of the disorder in the crystals. Simulated reciprocal space diffraction images show perfect ordering in the ab plane ($a = b \approx 3.94$ Å) and diffuse

Table 1. Composition-dependent unit-cell parameters of the $Ni_{3-x}GaTe_2$ (x = 0–1) series.

Batch starting composition	Refined a and c / Å	Cell volume / Å^3	Found composition (EDX)
Ni_2GaTe_2	3.9331(5), 15.923(2)	213.32(5)	$Ni_{2.3(1)}GaTe_{1.9(1)}$
$Ni_{2.25}GaTe_2$	3.9317(3), 15.927(1)	213.22(3)	$Ni_{2.35(7)}GaTe_{2.0(1)}$
$Ni_{2.3}GaTe_2$	3.9315(4), 15.926(1)	213.18(3)	$Ni_{2.35(5)}GaTe_{1.9(1)}$
$Ni_{2.5}GaTe_2$	3.9301(4), 15.909(1)	212.80(3)	$Ni_{2.5(1)}GaTe_{1.9(2)}$
$Ni_{2.75}GaTe_2$	3.9305(4), 15.852(3)	212.09(3)	$Ni_{2.7(1)}GaTe_{2.0(2)}$
Ni_3GaTe_2	3.933(1), 15.788(5)	211.50(6)	$Ni_{2.95(5)}GaTe_{2.0(2)}$

scattering in the perpendicular direction corresponding to the c axis. The SEM images of the crystal rims (Figure 2) clearly show the prominent layered character of the structure that makes stacking faults along interleaving 2D fragments highly probable. It is possible that because of the layered structure different crystals form agglomerates along [001] with a variable tilt around this direction.

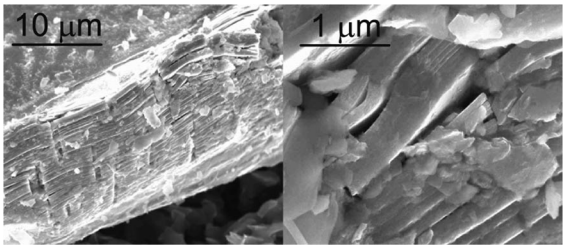

Figure 2. SEM images of Ni_3GaTe_2 crystals along the stacking direction. The intrinsic layered character of the structure is visible at higher magnification (right).

An intrinsic disorder of the structure must produce an increased diffuse background or, at least, reduced intensities of the Bragg reflections relative to an ordered sample. However, in our case the recorded XRD patterns show a smooth background, which indicates that structural disorder is not very likely. Because of the impossibility to obtain proper single crystals, the crystal structure of $Ni_{3-x}GaTe_2$ (x = 0, 0.25, 0.5) was refined from X-ray powder diffraction data by using the Rietveld method.

Crystal Structure Determination

The $Ni_{2.95}GeTe_2$ crystal structure[3] was chosen as a starting model for the Rietveld refinement for the Ni_3GaTe_2 compound. Preferred orientation along [001] was corrected by using the March–Dollase function. In the course of the crystal structure refinement, the occupational parameters of the Ni(2) and Ni(3) sites were allowed to vary, which finally led to the fractional occupancies given in Table 3. Individual isotropic displacement parameters were then refined for nickel and gallium atoms, and anisotropic ones for tellurium. The final cycles converged to the residuals of R_I = 0.042, R_p = 0.023, R_{wp} = 0.035. Experimental and calculated X-ray diffraction patterns, difference curve, and positions of calculated Bragg peaks are shown in Figure 3. Table 2 collects the crystallographic data and crystal structure refinement parameters for the new ternary nickel–gallium telluride. The positional and displacement parameters are listed in the Table 3. The resulting chemical composition $Ni_{2.98(1)}GaTe_2$ agrees well with the EDX analysis data (see previous section).

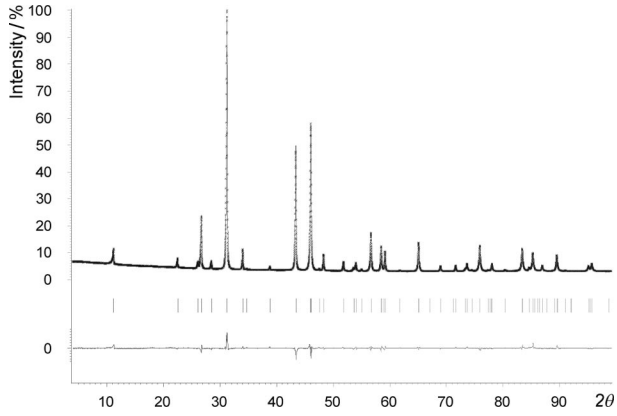

Figure 3. Observed, calculated and difference X-ray diffraction patterns for $Ni_{2.98(1)}GaTe_2$.

Table 2. Crystallographic data and the X-ray data collection and refinements statistics for $Ni_{2.98(1)}GaTe_2$.

Formula	$Ni_{2.98(1)}GaTe_2$
M_w / g mol^{-1}	500.8
Space group	$P6_3/mmc$ (No. 194)
Unit cell parameters / Å	a = 3.93933(3), c = 15.7933(2)
V / Å^3	212.250(3)
Z	2
T / K	293
$d_{calcd.}$ / g cm^3	7.82
2θ range / °	$4 < 2\theta < 100$
Refined atomic parameters	13
R_I, R_p, R_{wp}	0.042, 0.023, 0.035

Table 3. Fractional atomic coordinates, occupancies, and displacement parameters for $Ni_{2.98}GaTe_2$.

Atom	Wyckoff site	x/a	y/b	z/c	Occupancy	U_{iso} /Å^2
Ni(1)	4e	0	0	0.6694(1)	1	0.0251(5)
Ni(2)	2c	2/3	1/3	3/4	0.612(2)	0.0214(9)
Ni(3)	2a	0	0	1/2	0.372(3)	0.025(3)
Ga	2d	1/3	2/3	3/4	1	0.0401(7)
Te	4f	2/3	1/3	0.59048(5)	1	0.0192(3)[a]

[a] $U_{11} = U_{22} = 0.0067(3)$ Å^2, $U_{33} = 0.0442(6)$ Å^2, $U_{12} = 0.0033(1)$ Å^2, $U_{23} = U_{33} = 0$.

The layered Ni_3GaTe_2 structure (Figure 4) is based on $^2_\infty$[$Ni_{2.6}Ga$] slabs sandwiched along the c axis by two-atom-thick Te layers. Heterometallic slabs belong to a stuffed variant of the NiAs type, which is also referred to in the literature as defective Ni_2In type. The van der Waals gap is loosely filled by nickel atoms that occupy slightly more than

1/3 of the octahedral voids. The structure belongs to the $T_{3-x}MTe_2$ type (Figure 1b) and strongly resembles $Ni_{2.95}GeTe_2$[3] in terms of Ni(2) and Ni(3) site occupancy.

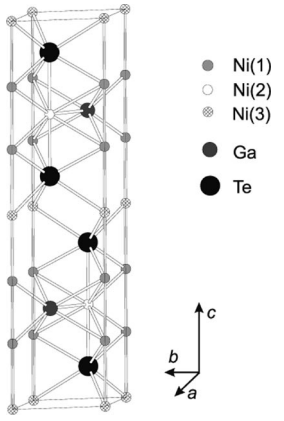

Figure 4. A view of the Ni_3GaTe_2 unit cell. Ni(2) and Ni(3) positions are shown as fully occupied.

Selected interatomic distances for Ni_3GaTe_2 are given in Table 4. The corresponding data for $Ni_{2.95}GeTe_2$ is also listed for comparison. Homo- and heterometallic bonds, Ni–Ni and Ni–M, are comparatively similar in both ternary nickel tellurides. It is also reasonable that the Ni(1)–Ga and Ni(1)–Te distances in ternary compounds resemble those in the Ni_2Ga structure[7] that adopts a Ni_2In-type structure [Ni(1)–Ga = 2.625 Å]. In contrast to the intermetallic compound, the octahedral first coordination sphere of Ni(1) is formed by three Ga and three Te atoms from the adjacent *hcp* array layers. The three Ga atoms, as equatorial vertices of the trigonal bipyramid base, and the two Te atoms, as the apical vertices of the trigonal bipyramid, constitute the coordination polyhedron for the Ni(2) atom. The rather short Ni(2)–Ga distance is also analogous to the same atomic contraction in Ni_2Ga, 2.311 Å. Such a short heterometallic bond is not very typical for this pair of elements, and this therefore gives a rationalization for the partial occupancy of the d-metal site. The Ni(3) coordination sphere is an octahedron formed by Te atoms only. The Ni–Te bonds in listed ternary compounds are similar to the typical atomic distances found in structures of numerous binary nickel tellurides, especially the $Ni_{1-x}Te$ solid solution, which represents a defective NiAs-type structure.

Table 4. Selected interatomic distances (Å) for the structures of $Ni_{2.98}GaTe_2$ and $Ni_{2.95}GeTe_2$.[3]

	$Ni_{2.98}GaTe_2$	$Ni_{2.95}GeTe_2$
M–Ni(1)	2.607(1)	2.619(1)
M–Ni(2)	2.274(1)	2.2574(6)
Ni(2)–Ni(1)	2.607(1)	2.619(1)
Te–Ni(2)	2.518(1)	2.6659(7)
Te–Ni(1)	2.592(1)	2.585(1)
Te–Ni(3)	2.687(1)	2.6659(7)
Ni(1)–Ni(1)	2.550(3)	2.656(4)

Further Rietveld structure refinements were performed for $Ni_{3-x}GaTe_2$ (x = 0.25, 0.5) by using the structural model described above. For x = 0.5, a minor Ni admixture (≈1%) was also taken into account. The final refined compositions are $Ni_{2.79(1)}GaTe_2$ and $Ni_{2.58(1)}GaTe_2$, respectively (see Table 5 for X-ray crystallographic data). Both phases adopt the same average crystal structure as Ni_3GaTe_2. Worth noting is a relatively constant occupancy of the Ni(3) site within the van der Waals gap of about 25–30%, which is accompanied by a decreasing occupancy of the Ni(2) site within a heterometallic fragment – it drops from 50% for $Ni_{2.79(1)}GaTe_2$ down to 36% for $Ni_{2.58(1)}GaTe_2$. Therefore, its magnitude is a major factor that determines the overall Ni content. The impossibility of the Ni(2) site to reach zero occupancy might be an explanation why it is not possible to produce compositions with a nickel content lower than in $Ni_{2.35}GaTe_2$. For $Ni_{3-x}GaTe_2$ (x = 0.7, 0.75) samples, a two-phase refinement was performed by taking Ga_2Te_3 admixtures (≈5%) into account, but the final residuals were even higher than for x = 0.5 and are therefore not given. Worth noting is that all peaks on these patterns were ascribed either to a Ni_3GaTe_2-like phase or to Ga_2Te_3. No superstructure reflections were observed.

Table 5. Refined crystallographic parameters for $Ni_{3-x}GaTe_2$ (x = 0.25, 0.5).

	$Ni_{2.79(1)}GaTe_2$	$Ni_{2.58(1)}GaTe_2$
a / Å	3.93190(2),	3.9291(2),
c / Å	15.8571(1)	15.9060(6)
Cell volume / Å^3	212.305(2)	212.65(2)
R_I, R_p, R_{wp}	0.053, 0.028, 0.039	0.081, 0.037, 0.056
z, Ni(1)	0.6699(1)	0.6712(2)
s.o.f.,[a] Ni(2)	0.500(3)	0.358(4)
s.o.f.,[a] Ni(3)	0.287(4)	0.224(5)
z, Te	0.59074(6)	0.59059(9)
U_{iso}, Ni(1) / Å^2	0.0316(4)	0.0351(6)
U_{iso}, Ni(2) / Å^2	0.0311	0.0351(6)
U_{iso}, Ni(3) / Å^2	0.0333	0.0351(6)
U_{iso}, Ga / Å^2	0.0466(7)	0.055(1)
U_{iso}, Te / Å^2	0.0280(3)	0.0268(5)

[a] s.o.f.: site occupancy factor.

The ED patterns along the main zone axes for Ni_3GaTe_2 are shown in Figure 5. The indexing based on the unit cell found by X-ray diffraction convincingly correlates with the proposed crystal symmetry and lattice parameters. Systematic extinction conditions are in accordance with the space group $P6_3/mmc$. The presence of forbidden 00l, $l \neq 2n$, reflections on [010] and [1$\bar{1}$0] patterns is caused by double diffraction as was verified by the tilting of the crystallite along the [001] direction. With reference to the literature,[6] the structure can be regarded as a commensurately modulated supercell of the NiAs-type subcell with a modulation vector $\boldsymbol{q}$ = 2/3c*. Thus, the brighter spots along the [001] direction on the [010] and [1$\bar{1}$0] zone patterns correspond to a NiAs-type subcell with $c \approx 5.4$ Å, while the weaker spots in between reflect a superstructure, which manifests itself in a regular alternation of heterometallic Ni/Ga and Ni/Te two-dimensional slabs along the c axis in a 1:1 ratio. The perfect ordering of the slabs is confirmed by HRTEM (Figure 6). The dark regions correspond to the atoms (high-projected potential), while the bright spots reflect cavities

(low-projected potential). The Fourier transform shown in Figure 6 agrees with the experimental ED pattern of the [1$\bar{1}$0] zone.

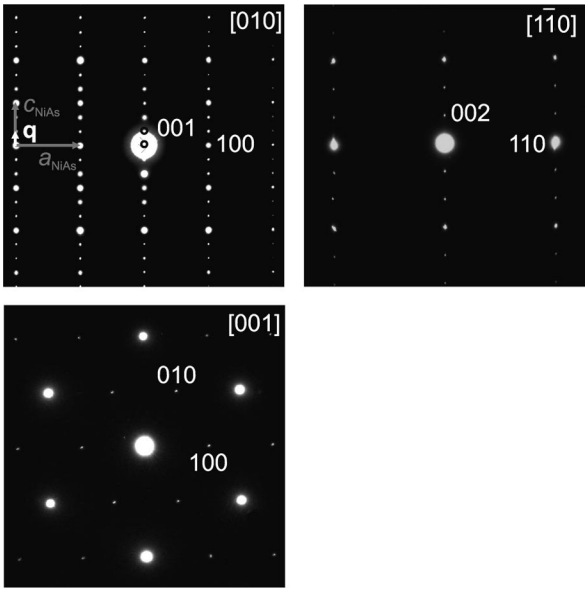

Figure 5. Main zone electron diffraction patterns for Ni_3GaTe_2.

Figure 6. Theoretical (f = –35 nm, t = 12 nm, dashed outline) and experimental [1$\bar{1}$0] zone HRTEM image of Ni_3GaTe_2. The corresponding Fourier transform is shown as an inset. A solid line outlines the unit cell.

The [010] and [1$\bar{1}$0] ED patterns recorded on a FIB lamella cut from a Ni_3GaTe_2 crystal coincide with those described above and therefore confirm that the strong disorder observed in the X-ray single-crystal experiments is most likely caused by an agglomeration of single crystals and does not originate from a structural disorder of the layers at a unit cell level. Further, no diffuse intensities observed for $Ni_{2.95}GeTe_2$[3] and attributed to different types of intrinsic structural disorder or Moiré effects were detected in our samples.

An example of In-containing mixed tellurides[6] shows that the ordering of 2D slabs depends on the nickel content, which affects the magnitude of the modulation wave vector ***q*** and, consequently, the unit cell parameter c. Therefore, an electron microscopy study of Ni-poor samples $Ni_{2.79(1)}GaTe_2$, $Ni_{2.58(1)}GaTe_2$, and $Ni_{2.35}GaTe_2$ (from here on this composition is assigned according to the EDX data) was carried out. No evidence towards any change in slab-stacking sequence along the c axis was found. The ED patterns of $Ni_{2.79}GaTe_2$ are similar to those of Ni_3GaTe_2, while the two other phases reproducibly display an additional ordering in the ab plane with $a_{sup} = b_{sup} = 2a_{sub} \approx 7.8$ Å (Figure 7 for the $Ni_{2.58}GaTe_2$ patterns; $Ni_{2.35}GaTe_2$ has similar ED patterns). The symmetry of the unit cell remains unchanged; this is evident from the reflection conditions corresponding to the space group $P6_3/mmc$. Despite careful X-ray powder diffraction studies, no superstructure reflections could be detected in the XRD patterns of Ni-poor samples; this is likely due to the rather small size of the domains, which leads to diffuse X-ray superstructure peaks.

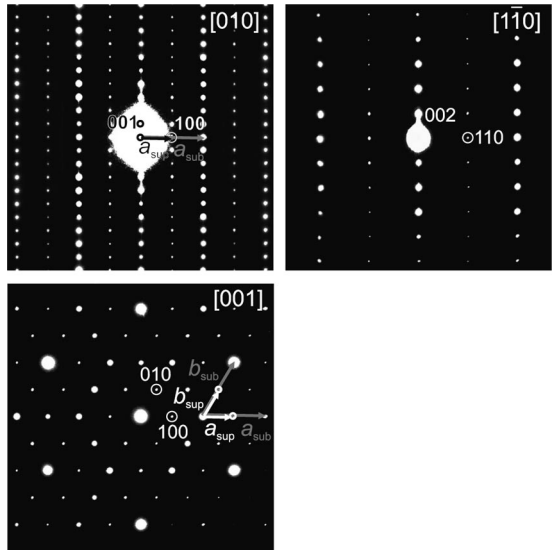

Figure 7. Main zone electron diffraction patterns for $Ni_{2.58}GaTe_2$. a_{sub} and b_{sub} correspond to the unit-cell parameters for Ni_3GaTe_2.

As no ordering appears along the c axis, the only remaining possibility is an ordering of Ni atoms and vacancies in the ab plane. Given the fact that the superstructure stabilizes with minor amounts of Ni and by taking into account that only the Ni(2) site occupancy is significantly reduced when the overall nickel content decreases, the primary suggestion is that the ordering takes place in the heterometallic fragments. The geometry of the heterometallic slabs in the ternary compounds of the $Ni_{3-x}MTe_2$ type is closely related to the structure of the corresponding binary intermetallics. Therefore, it seems reasonable to search for a similar superstructure among known structures of d-metal–p-metal intermetallics that are derivatives of the NiAs type. The only similar superstructure with $a_{sup} = b_{sup} = 2a_{NiAs}$, $c_{sup} = c_{NiAs}$ is adopted by $Fe_{2-x}Ge$.[8] The doubling of the unit cell parameters in the ab plane reflects the ordering of the Fe atoms and vacancies that occurs in a site similar to T(2) in the $T_{3-x}MTe_2$-type structure: 1/4 of the Fe(2) atoms are regularly missing in the ideal $Fe_{1.75}Ge$ superstructure. But the $Fe_{2-x}Ge$ phase has a homogeneity range 60–63 at.-% Fe,[9] therefore, its composition changes from $Fe_{1.5}Ge$ to Fe_2Ge, which corresponds to 67 and 100%

occupancy of the Fe(2) site, respectively. The ordered superstructure with doubled *a* and *b* unit-cell parameters is reported for 83% of the Fe(2) site occupancy. On the basis of this, one can expect that this vacancy ordering will take place over a certain compositional range, even when the ratio vacancy/occupied site deviates from 1:3.

Taking these considerations into account, we assumed that the heterometallic slabs in Ni-poor $Ni_{3-x}GaTe_2$ ($0.5 \leq x \leq 0.65$) structures might represent 2D cuts from the hypothetical intermetallics structure in which d-metal atoms and vacancies are distributed in a reverse order relative to those in the $Fe_{1.75}Ge$-type structure. The constructed structural model of the ternary phase is presented in Figure 8a. In the supercell with doubled *a* and *b* unit-cell parameters, the former Ni(2) site in a heterometallic slab splits into two sites: Ni(2)′ (site symmetry 2*c*) and Ni(2)′′ (site symmetry 6*h*). In the proposed model, the first position is occupied, while the second remains vacant, which gives rise to the composition $^{2}_{\infty}[Ni_{2.25}Ga]$ for the heterometallic fragment.

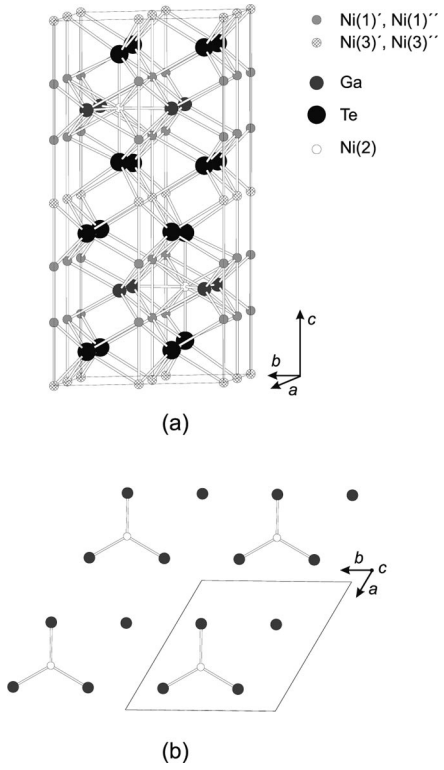

Figure 8. (a) A view of the unit cell for the model $Ni_{3-x}GaTe_2$ compound with superstructure $a_{sup} = b_{sup} = 2a_{sub}$. 3/4 of the atoms are regularly missing in the Ni(2) site in contrast to that in Ni_3GaTe_2. The Ni(3)′ and Ni(3)′′ positions are shown as fully occupied; (b) Ni(2) and Ga atom ordering in the *ab* plane (2D cut of a single heterometallic slab).

With an occupancy of the Ni site in the van der Waals gap of ca. 30% (according to Rietveld refinements), we estimate that the ideal composition is close to $Ni_{2.55}GaTe_2$; this is in reasonable agreement with the upper limit of the composition range in which the superstructure has been identified. The occupancy of the nickel site within the van der Waals gap is assumed to be constant, while in the real structure it may vary and hence change the ratio between the occupancies of the two d-metal sites and the overall Ni content.

Since it was not possible to refine the superstructure with X-ray powder diffraction data, we have conducted HRTEM studies on the most Ni-poor sample (Figure 9). Simulated HRTEM images were calculated for model compounds with different types of vacancy ordering in partially occupied Ni sites. Only two options were in a good agreement with the experimental images for $Ni_{2.35}GaTe_2$: when $Fe_{1.75}Ge$-like heterometallic slabs or slabs with a reversed occupancy pattern of d-metal atoms and vacancies and loosely filled van der Waals gaps are simulated (see Figure 9). By taking the low Ni content into account, the proposed model of the Ni(2) atoms and the vacancies distribution is thus confirmed. HRTEM image simulations for other possible ordering patterns confirm that the experimentally observed contrast cannot be created by Ni-atom ordering in the van der Waals gap.

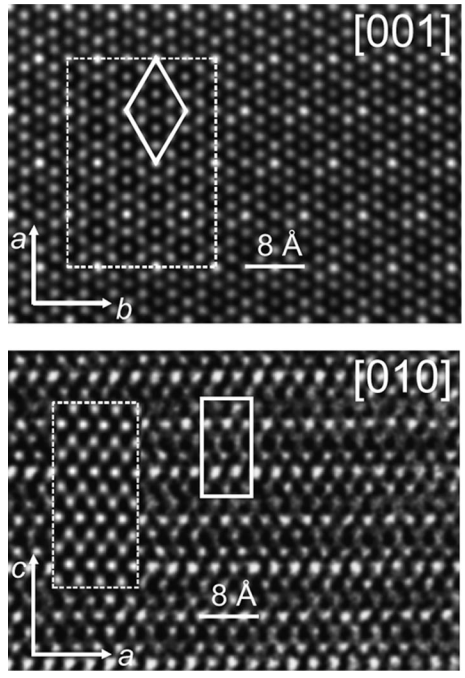

Figure 9. Theoretical ($f = -35$ nm, $t = 3.5$ nm, dashed outline) and experimental [001] HRTEM image of $Ni_{2.35}GaTe_2$ (top). The solid line outlines the unit cell with $a \approx 7.9$ Å. Theoretical ($f = -12$ nm, $t = 2$ nm, dashed outline) and experimental [010] HRTEM image of $Ni_{2.35}GaTe_2$ (bottom). The solid outline corresponds to the unit cell with $a \approx 7.8$ Å, $c \approx 16$ Å.

In the experimental [001] HRTEM image (see Figure 9a), brighter dots in the rhomb vertices correspond to Ni-atom rows that build the NiAs-type framework. Each light grey dot in the center of the rhomb represents another pure Ni-atom row surrounded by six grey spots. The two darker dots, above and below the rhomb center, correspond to

mixed Ni/Ga/Te atom rows in which extra Ni(2)′ atoms are found. The four lighter spots in the hexagonal arrangement correspond to mixed Ga/Te rows in which the d-metal sites are vacant.

The [010] experimental and simulated HRTEM images do not give any additional insight because the structural features under consideration contribute only very slightly to the observed contrast and may only be noticed as a slight modulation of the dot intensities along the *a* axis.

The in-plane distribution of the Ni(2) and Ga atoms (see Figure 8b) stabilized in the superstructure is most likely aimed to relax the structural strain, because it enables atomic displacements of Ga towards the vacant sites and an elongation of the very short Ni(2)–Ga distances. The proposed ordering can only occur for low Ni(2) site occupancies, therefore, it is not observed for densely occupied sites in $Ni_{2.79}GaTe_2$ and Ni_3GaTe_2.

On the other hand, a total absence of Ni(2) atoms seems to be impossible, and the series of compounds $Ni_{3-x}GaTe_2$ has a compositional range limit of $x \approx 0.65$. The reason may be found in a mutual adjustment of the 2D heterometallic slabs and the Ni/Te fragments in the *ab* plane that requires a certain expansion of the Ni/Ga slab, which can be achieved by adding extra Ni(2) atoms.

Band Structure and Physical Properties

The model unit cells used for the calculations of $Ni_{2.25}GaTe_2$ and $Ni_{2.75}GaTe_2$ compositions correspond to the new superstructure of $Ni_{3-x}GaTe_2$ (Figure 8a) and a hypothetical superstructure with Ni atom/vacancy occupancy in Ni(2) site corresponding to the $Fe_{1.5}Ge$-type structure.

Figure 10 shows the total and projected density of states (DOS) near the Fermi level for all four models, and Figure 11 shows the band structure for Ni_2GaTe_2 and Ni_3GaTe_2. The rest of the band structures appear to be quite similar to that of Ni_3GaTe_2.

Quantum chemical data suggest metallic conductivity for all the compositions, as evident from the low but non-zero density of states at the Fermi level. The main contribution to the DOS near the Fermi level arises from the nickel 3d-states that are almost filled. Tellurium 5p-states appear in the same energy range, but their density is much lower, while the gallium states contribute even less. The almost filled nickel states also suggest a Pauli-like paramagnetic behavior for all the investigated compounds. Calculated Mulliken charges are given in Table 6.

The band structure near the Fermi level indicates a possibility of anisotropy because of the different number of bands crossing the Fermi level along the different directions, albeit, according to the DOS calculations, all the model compounds are three-dimensional metallic conductors. Nevertheless, spatial differences in the bonding nature may produce a certain anisotropic behavior and affect the electrical properties. This is confirmed by the anisotropy of the electrical resistivity measured in two perpendicular directions for pressed textured pellets of Ni_3GaTe_2 (Figure 12). The $\rho_\perp/\rho_\parallel$ ratio is 2 ($\rho_\parallel$ – electrical resistivity along the heterometallic fragments, $\rho_\perp$ – electrical resistivity perpendicular to the heterometallic fragments).

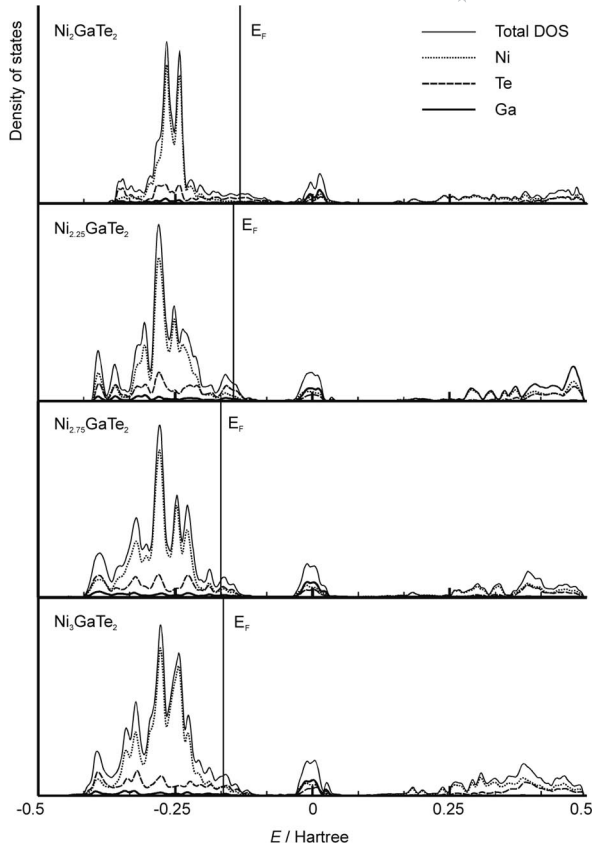

Figure 10. Total and projected densities of states for $Ni_{3-x}GaTe_2$.

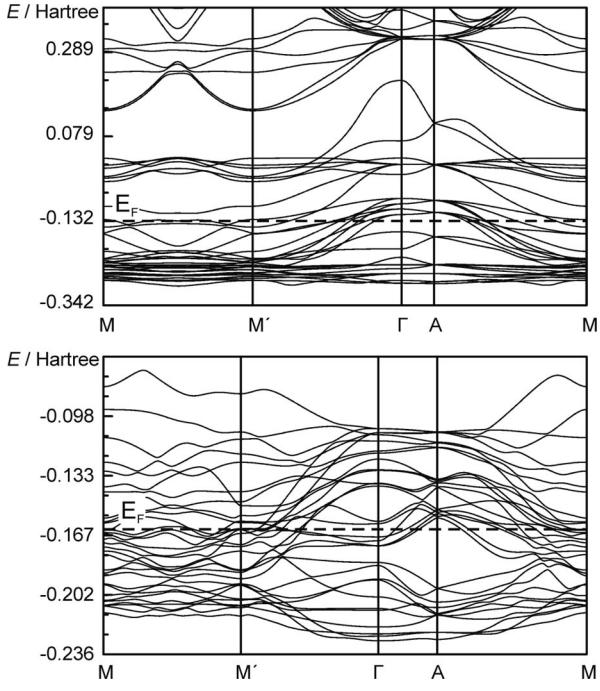

Figure 11. Band structure near the Fermi level for Ni_2GaTe_2 (above) and Ni_3GaTe_2 (below).

Table 6. Calculated Mulliken charges for $Ni_{3-x}GaTe_2$ (x = 1, 0.75, 0.25, 0).

	Ni_2GaTe_2	$Ni_{2.25}GaTe_2$	$Ni_{2.75}GaTe_2$	Ni_3GaTe_2
Ga	+0.94	+0.85	+0.99	+0.92
		+0.99	+1.13	+1.15
Te	–0.65	–0.54	–0.45	–0.49
		–0.56	–0.37	–0.44
Ni	+0.18	+0.24	+0.41	+0.31
		+0.17	+0.38	+0.39

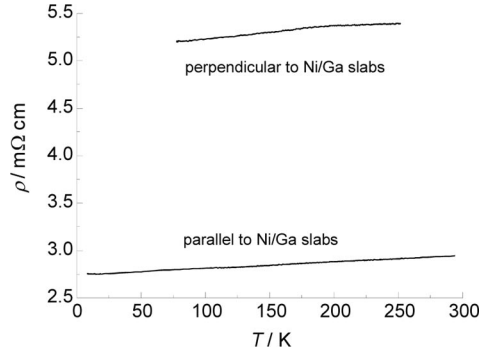

Figure 12. Temperature dependence of the electrical resistivity for perpendicular crystallographic directions for the Ni_3GaTe_2 pellet.

The experimentally measured temperature dependence of the magnetic moment points towards a weak temperature-independent Pauli-like paramagnetism that agrees with the results of the quantum chemical calculations. Figure 13 shows the temperature dependence of product χT for Ni_3GaTe_2. The experimental data may be approximated by the dependence $\chi = \chi_0 + C\cdot(T+\theta)^{-1}$, where $\chi_0 = 2.37\times10^{-7}$ emu g^{-1} Oe^{-1}, $C = 4.83\times10^{-6}$ emu K g^{-1} Oe^{-1}, and θ = +1.1 K (solid line in Figure 13). The increasing magnetic susceptibility below 50 K may be attributed to slight traces of paramagnetic impurities, well below the detectable level for the X-ray or EDX analysis. The effective magnetic moment μ_{eff} for this Curie–Weiss contribution, determined from the Curie constant $C = \mu_{eff}^2(3k)^{-1}$, has the value 0.12 μ_B per formula unit.

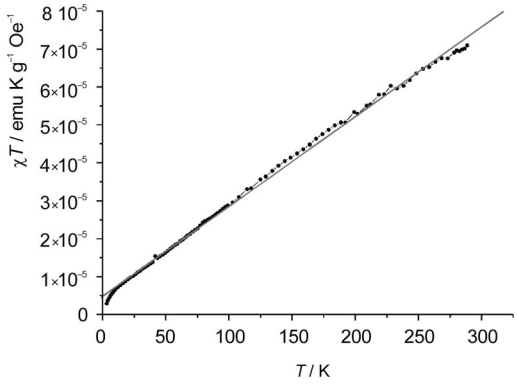

Figure 13. The temperature dependence of χT for Ni_3GaTe_2 and a linear fit according to the Curie–Weiss law.

In order to explore the thermal stability of Ni_3GaTe_2, DSC experiments were performed. The heating curve of the sample shows a strong endothermic effect at 965 °C. According to the X-ray powder diffraction data, a partially molten sample after the DTA experiment contains the title compound only. This result confirms the suggestion that Ni_3GaTe_2 melts congruently at the registered temperature.

Conclusions

We would like to emphasize the close relationship between the structures of mixed nickel (iron)–main group metal layered tellurides of the $T_{3-x}MTe_2$ type. In all the structures, the octahedral and trigonal-bipyramidal voids within the ordered M/Te hexagonal close packing are selectively filled by d-metal atoms T. The occupancy and ordering pattern of filled and vacant voids are affected by the type of p-element coordination shell that surrounds them. The octahedral voids that have a mixed M/Te environment are always completely occupied and form a two-dimensional T/M fragment of the NiAs type. In the resulting T_2MTe_2 structure, two types of sites remain, denoted **A** (within the heterometallic slab) and **B** (within the van der Waals gap); they have trigonal-bipyramidal and octahedral coordination polyhedra, respectively (see Figure 1b). They can be fractionally occupied by extra d-metal atoms to give an overall composition $T_{3\pm x}MTe_2$. The two-dimensional heterometallic fragment with partially occupied **A** sites belongs to a defect Ni_2In type that can also be considered as a stuffed NiAs type. The end-member in which both **A** and **B** sites are fully occupied would have the composition T_4MTe_2, but no evidence of the existence of such a compound has been found so far. The composition Ni_2MTe_2 reported for only M = Sb[2] to date corresponds to the complete absence of additional atoms in both **A** and **B** sites (see Figure 1a).

For the Ni-rich $Ni_{3\pm x}InTe_2$ and $Ni_{3-x}SnTe_2$ composition, a non-zero occupancy of both atomic positions has been detected.[4–6] In these compounds, the van der Waals gap is densely occupied in contrast to that in the heterometallic Ni/M fragment. This fact is easily rationalized by a similarity of the In/Sn and Te atomic radii, which provides much more free space in the gap relative to a trigonal-bipyramidal void in a heterometallic slab. The large radii of these p-elements provide bigger **A** and **B** voids, so the occupancy of both sites is quite high. In the case of In,[6] the overall nickel content in the composition formula may even exceed 50 at.-%, e.g. $Ni_{3.32}InTe_2$. Worth noting are the incommensurate and commensurate structural modulations for the In-containing compounds,[6] which are closely related to a variable nickel content and fractional occupancy of the sites discussed. The modulation vector has non-zero components only along the c axis and its magnitude varies with changing Ni content. The incommensurate modulation affects the stacking sequence of the heterometallic Ni/In slabs and the Ni-filled van der Waals gaps that becomes aperiodic in 3D space; four or even more predominantly Te layers can fol-

low each other in an *hcp* array. This model evidently leads to variations in the In/Te ratio, but it is assumed in[6] that both In and Te can be partially intermixed at their sites in the *hcp* array, thus smoothing away the effect on the overall composition.

Germanium and gallium appear to be the only rather small p-elements involved in this structure type. Their size gives rise to the structural peculiarity that **A**-type voids are preferably occupied, while **B**-type voids remain vacant to a large extent. Moreover, the unique ternary iron-containing telluride exists for germanium. The present contribution reveals an extended homogeneity range for the $Ni_{3-x}GaTe_2$ phase, comparable to that for the In-containing compound. It is worth noting that the type of superstructure changes drastically as Ga substitutes In; ordering occurs within the heterometallic slabs and leads to an ordering of the Ni atoms in the partially occupied sites. This structural feature, however, cannot be generalized for both "light" p-elements, since the fine structural aspects have not yet been investigated for Ge-containing compounds and no data about any possible superstructure or large d-metal homogeneity ranges have been reported. Since extra d-metal atoms are mostly missing in the van der Waals gap for mixed d-metal–germanium and d-metal–gallium tellurides, the latter can be considered to be layered compounds, as evidenced by a higher anisotropy of their physical properties. They possess well-defined 2D-extended regions of intensive T/Ge bonding spatially separated from each other along the *c* axis by regions of weak electrostatic van der Waals interactions.

The analysis of our results along with the published data shows that the distribution of extra d-metal atoms between the two partially occupied **A** and **B** voids depends on the chemical nature and radius of the p-element involved. As the Ni content increases, the filled and vacant voids in the heterometallic slabs and in the van der Waals gap are not distributed at random, and ordering patterns differ significantly for the compounds containing "heavy" and "light" p-elements. This aspect is promising from the viewpoint of potential anisotropy applications.

Experimental Section

Synthesis, Preliminary Sample Characterization and Crystal Growth: Thoroughly ground mixtures of the elements (ca. 1 g in total) that correspond to the compositions Ni_2MTe_2 and Ni_3MTe_2 (M = Al, Ga, Si, As) were sealed under vacuum ($\approx 5 \times 10^{-2}$ Torr) in silica ampoules, annealed at various temperatures within the temperature range 720–750 °C for 5–10 d, and then allowed to cool down to room temperature. The Ni powder (99.8%) was preheated at 500 °C under a hydrogen stream flow for 4 h in order to purify it from nickel oxide contamination prior to its use, As (99.9%) powder purification was accomplished by heating with a strong potassium dichromate solution for 1 h, and the remaining elements, all 99.99% pure, were used as purchased.

Following the results of the X-ray analysis of annealed samples, additional compounds with the composition $Ni_{3-x}GaTe_2$ (x = 0.75, 0.7, 0.5, and 0.25) were synthesized by annealing at 750 °C for 14–20 d. It has been reported[10] that phase equilibria are very difficult to reach in the Ni–Si–Q (Q = S, Se, Te) systems if mixtures of the elements are used as starting reagents. Therefore, additional attempts to prepare Si-containing compounds from a mixture of presynthesized Ni_3Si, Ni, and Te were undertaken. The compositions of the products were studied by X-ray powder diffraction (Nonius FR-551 Guinier camera, Cu-$K_{\alpha 1}$). EDX analysis was carried out with a Jeol JSM-5510 scanning microscope with an Inca+ Energy attachment. Samples were analyzed by using the Ni-K_α, Ga-K_α, and Te-L_α lines. Pure nickel metal, GaP, and HgTe were used as primary standards. The data were averaged from 10–15 spots on flat surfaces of each crystallite. The maximum error of the determination was 2 at.-%.

Attempts to grow single crystals by using different flux materials, such as NaCl, KI, KBr, and KCl, were undertaken. Stoichiometric mixtures of the elements that correspond to the ternary compound (ca. 1 g in total) and flux salt (ca. 1 g, dried by heating at 400 °C for 1 d prior to use) were placed into dried silica ampoules, evacuated, and sealed under a dynamic vacuum. The ampoules were then heated up to 910 °C over 12 h, annealed at that temperature for another 12 h, cooled down to 800 °C at a rate of 1 °C/h, then at a rate of 2 °C/h down to 670 °C, and finally allowed to cool down to room temperature. The flux was removed by boiling in distilled water. A crystal growth experiment without flux was also pursued. The stoichiometric mixture of the elements was preheated at 750 °C for 5 d and then slowly cooled down to 350 °C at a rate of 2 °C/h. Crystals of better quality were obtained by using the molten flux route; however, none of them turned out to be suitable for a single-crystal X-ray analysis.

Further details of the crystal structure investigation on the new ternary nickel–gallium tellurides can be obtained from the Fachinformationszentrum Karlsruhe, 76344 Eggenstein-Leopoldshafen, Germany [Fax: (+49)7247-808-666; E-mail: crysdata@fiz-karlsruhe.de] on quoting the depository number CSD-421061 ($Ni_{2.98(1)}GaTe_2$), -421062 ($Ni_{2.79(1)}GaTe_2$), and -421063 ($Ni_{2.58(1)}GaTe_2$).

X-ray and Electron Microscopy Studies: The X-ray diffraction powder data were collected on a Huber G670 diffractometer (Cu-$K_{\alpha 1}$ radiation, Ge monochromator, transmission mode). The crystal structures of Ni_3GaTe_2, $Ni_{2.79}GaTe_2$, and $Ni_{2.58}GaTe_2$ were refined by using the full-profile Rietveld method (JANA2000 program package[11]).

Samples for electron microscopy were prepared by grinding phase-pure polycrystalline samples in ethanol within an agate mortar and by deposing fragments on a holey carbon grid. Electron diffraction (ED) and high-resolution transmission electron microscopy (HRTEM) studies were performed on a Philips CM20 and a Tecnai G2 (200 kV, FEG) microscope. Image simulations were made with the CrystalKit and MacTempas software.[12]

The FIB (focused ion beam) work was performed on Ni_3GaTe_2 crystals by using a FEI-NanoLab Nova 200 dual beam system. FIB milling was performed by using an ion beam of 30 kV for all steps, except for the final cleaning, where an energy of 5 kV was used.

Differential Scanning Calorimetry: The thermal analysis was performed by using a NETZSCH STA 409 PC device in a 30–1000 °C temperature range on a pure Ni_3GaTe_2 sample (ca. 50 mg) placed in a corundum crucible under a flow of dry argon (40 mL/min). The heating curve was registered in an automated mode at a heating rate of 10 °C/min. The temperature measurement error did not exceed ±2 °C. The sample weight difference error with respect to an empty crucible did not exceed 10^{-6} g.

Quantum Chemical Calculations: Ab initio electronic structure calculations on the model compounds Ni_2GaTe_2, $Ni_{2.25}GaTe_2$,

$Ni_{2.75}GaTe_2$, and Ni_3GaTe_2 were performed by using the DFT approach (CRYSTAL98 program package[13]). The structure models were constructed within an assumption of vacant Ni(2) and Ni(3) sites (see Table 3 for labels of atomic sites) for Ni_2GaTe_2 and of fully occupied and vacant Ni(2) and Ni(3) sites for Ni_3GaTe_2, respectively. A simulation of the ordered $Ni_{2.25}GaTe_2$, $Ni_{2.75}GaTe_2$, and Ni_3GaTe_2 compositions required a quadruple unit cell with respect to the original cell, with doubled *a* and *b* values (see "Crystal Structure Determination" subsection). Hay–Wadt effective core potentials (large-core pseudopotential for Ga and Te; small-core pseudopotential for Ni) and corresponding valence basis sets,[14] modified for calculations of solids, were used in the calculations by employing the B3LYP Hamiltonian. Basis sets were tested by calculating band structures of metals and binary chalcogenides and were found to be suitable for an adequate representation of the main features of their electronic structure and bonding. In each case, 300 *k*-points were used for the band structure calculations. Each calculation included a converged SCF (self-consistent field) run. The convergence criterion for the SCF energy was set to 10^{-7} Hartree.

Acknowledgments

The authors are grateful to Prof. P. E. Kazin (Moscow State University, Russia) for magnetic property measurements. We are indebted to S. Van den Broeck (University of Antwerp, Belgium) for FIB sample preparation and to Dr. V. G. Kytin and Prof. V. A. Kulbachinskii (Moscow State University, Russia) for electrical conductivity measurements. A. I. acknowledges the Belgian Science Policy (BELSPO) for a postdoctoral grant during her stay at the University of Antwerp. This work was supported by the Russian Foundation for Basic Research (grant No. 09-03-12296-ofi_m) and the Presidential Programme of the Russian Academy of Sciences (grant 18P22).

[1] a) S.-T. Hong, J. D. Martin, J. D. Corbett, *Inorg. Chem.* **1998**, *37*, 3385–3390; b) P. A. Maggard, J. D. Corbett, *J. Am. Chem. Soc.* **2000**, *122*, 10740–10741; c) A. I. Baranov, L. Kloo, A. V. Olenev, B. A. Popovkin, A. I. Romanenko, A. V. Shevelkov, *J. Am. Chem. Soc.* **2001**, *123*, 12375–12379; d) M. Ruck, *Angew. Chem. Int. Ed.* **2001**, *40*, 1182–1193; e) A. I. Baranov, A. A. Isaeva, L. Kloo, B. A. Popovkin, *Inorg. Chem.* **2003**, *42*, 6667–6672; f) A. I. Baranov, L. Kloo, A. V. Olenev, B. A. Popovkin, A. I. Romanenko, *Inorg. Chem.* **2003**, *42*, 3988–3993.
[2] T. K. Reynolds, R. F. Kelley, F. J. DiSalvo, *J. Alloys Compd.* **2004**, *366*, 136–144.
[3] H.-J. Deiseroth, K. Aleksandrov, C. Reiner, L. Kienle, R. K. Kremer, *Eur. J. Inorg. Chem.* **2006**, *8*, 1561–1567.
[4] O. N. Litvinenko, A. N. Kuznetsov, A. V. Olenev, B. A. Popovkin, *Russ. Chem. Bull.* **2007**, *56*, 1945–1947.
[5] H.-J. Deiseroth, F. Sprirovski, C. Reiner, M. Schlosser, *Z. Kristallogr. – New Cryst. Struct.* **2007**, *222*, 169–170.
[6] a) A.-K. Larsson, L. Norén, R. L. Withers, H. Rundloef, *J. Solid State Chem.* **2007**, *180*, 2723–2733; b) L. Norén, R. L. Withers, F. Brink, *J. Alloys Compd.* **2003**, *353*, 133–142.
[7] E. Hellner, *Z. Metallk.* **1950**, *41*, 480–484.
[8] S. Lidin, A.-K. Larsson, *J. Solid State Chem.* **1995**, *118*, 313–322.
[9] J. Maier, E. Wachtel, *Z. Metallk.* **1972**, *63*, 411.
[10] A. A. Isaeva, A. I. Baranov, Th. Doert, M. Ruck, V. A. Kulbachinskii, R. A. Lunin, B. A. Popovkin, *Russ. Chem. Bull.* **2007**, *56*, 1694–1700.
[11] V. Petricek, M. Dusek, L. Palatinus. *Jana2000 – The Crystallographic Computing System*, Institute of Physics, Praha, Czech Republic, **2000**.
[12] *CrystalKitX and MacTempas Software Packages for High Resolution Electron Microscopy*, Total Resolution, Berkeley, CA, USA.
[13] V. R. Saunders, R. Dovesi, C. Roetti, M. Causà, N. M. Harrison, R. Orlando, C. M. Zicovich-Wilson, *CRYSTAL98 User's Manual*, University of Torino, Torino, **1998**.
[14] a) for Ni: F. Freyria-Fava, Ph.D. Thesis, University of Torino, Torino, **1997**; b) for Ga, Te: P. J. Hay, W. R. Wadt, *J. Chem. Phys.* **1985**, *82*, 284–298.

Received: October 23, 2009
Published Online: February 12, 2010

